

Application of a fixed Eulerian mesh-based scheme based on the level set function generated by virtual nodes to large-deformation fluid-structure interaction

Gaku Hashimoto*¹, Kenji Ono² and Hiroshi Okuda³

¹The University of Tokyo, 7-3-1 Hongo, Bunkyo-ku, Tokyo 113-8656, Japan

²RIKEN, 7-1-26 Minatojima-minami-machi, Chuo-ku, Kobe, Hyogo, 650-0047 Japan

³The University of Tokyo, 5-1-5 Kashiwanoha, Kashiwa, Chiba 277-8568, Japan

(Received February 1, 2012, Revised July 18, 2012, Accepted September 2, 2012)

Abstract. We apply a partitioned-solution (iterative-staggered) coupling method based on a fixed Eulerian mesh with the level set function to a large-deformation fluid-structure interaction (FSI) problem where a large-deformable thin structure moves in a high-speed flow field, as an airbag does during deployment. This method combines advanced fluid and structure solvers—specifically, the constrained interpolation profile finite element method (CIP-FEM) for fluid Eulerian mesh and large-deformable structural elements for Lagrangian structural mesh. We express the large-deformable interface as a zero isosurface by the level set function, and introduce virtual nodes with level sets and structural normal velocities to generate the level set function according to the large-deformable interfacial geometry and enforce the kinematic condition at the interface. The virtual nodes are located in the direction normal to the structural mesh. It is confirmed that application of the method to unfolded airbag deployment simulation shows the adequacy of the method.

Keywords: fluid-structure interaction; large deformation; Eulerian mesh; level set function; interface treatment; partitioned-solution method.

1. Introduction

Highly accurate analyses of mechanical interactions such as fluid-structure interactions (FSI) are important for elucidating complex physical phenomena in fields such as automotive engineering, civil engineering, aerodynamics and biomechanics. Various FSI simulation methods have been recently developed and applied (see Bungartz and Schafer 2007).

This study describes application of a FSI simulation method to large-deformation FSI problems such as airbag deployment simulations where accurate simulation is necessary for human safety. Airbag deployment is one of the coupled problems of inviscid compressible air flow and thin elastic structure. After car impact, high-speed air flow, with high density and high pressure, enters a folded airbag rapidly and inflates it due to aerodynamic force. The inflation causes rapid pressure variation

* Corresponding author, Research Associate, E-mail: gashimoto@sys.t.u-tokyo.ac.jp

of the interior domain of the airbag and the rapid exterior pressure variation might result in passenger's eardrum-splitting.

Today, commercial crash-simulation software packages such as LS-DYNA, PAM-CRASH and MADYMO are widely used for developing airbags, including frontal, side, knee and rear airbags, as shown in Souli and Olovson (2003), Zhang *et al.* (2004), Mahangare *et al.* (2005) and Ruff *et al.* (2006). Many early simulations used the uniform pressure method (UPM), where the pressure on the inside of an airbag is assumed to be uniform and the airbag is assumed to be sufficiently inflated when it comes in contacts with a passenger. However, it is also necessary to protect a passenger seated near an insufficiently inflated airbag, in an unsafe state called "out-of-position (OoP)". To address this need, more recent simulations compute the pressure on the inside of the airbag by using computational fluid dynamics (CFD), which has been now introduced to commercial software.

Along this line, we have been investigating fluid-structure coupling methods that are robust and accurate for solving large-deformation FSI problems. For this study, we need to select either the moving arbitrary Lagrangian-Eulerian (ALE) mesh-based scheme or the fixed Eulerian mesh-based scheme. In the moving ALE mesh-based scheme, used frequently in research and commercial application such as LS-DYNA (see Wall and Ramm 1998, Rugonyi and Bathe 2001, Zhang and Hisada 2001, Ishihara and Yoshimura 2005), fluid nodes exist on the interface and must move according to the motion of the structure. It is necessary to control the movement of the fluid nodes or change the connectivity between them so as not to distort the ALE mesh during computation. However, when the scheme is applied to large deformation FSI problems, remeshing and mesh-control markedly increase computational time. The scheme therefore tends to need computational cost for large-deformation FSI problems. On the other hand, in the fixed Eulerian mesh-based scheme, the fluid mesh overlaps the structural mesh and fluid nodes do not necessarily exist on the interface. It is necessary to satisfy the kinematic condition that the fluid and structural normal velocities match at the interface. In many applications of this scheme, a fictitious fluid domain is defined by immersing a fluid in a structural domain embedded in a fluid domain. The fluid velocity in the fictitious fluid domain is assumed to be equal to the structural velocity. If the fluid is incompressible, the structure is also incompressible. The immersed boundary (IB) method of Peskin and McQueen (1989) is a representative fixed Eulerian mesh-based scheme. In the IB method, a structure has no volume and the motion effect of the structure is introduced to the equations of motion for a fluid as an interaction force. Since the frequency of a flexible structure is relatively small, the IB method is suitable for use with flexible rather than industrial structures. For example, an airbag is one of the industrial structures and the Young's modulus is on the order of 10^9 Pa, hundreds or thousands of times larger than that of the living body wall. The extended IB method (EIBM) of Wang and Liu (2004) and the immersed finite element method (IFEM) of Zhang *et al.* (2004) have recently been developed as IB methods for use with structures occupying finite volumes in a fluid domain. Sawada and Hisada (2005) stabilized the IB method by defining a structural domain and fluid subdomain near the structure as a fictitious domain. The distributed Lagrange multiplier/fictitious domain (DLM/FD) method of Glowinski *et al.* (1998) is similar to the IB method. The DLM/FD method was originally applied to FSI problems of fluids and rigid bodies by Glowinski *et al.* (1998) and has been recently applied to FSI problems of fluids and elastic structures by Baajiens (2001).

In this study, we apply a partitioned-solution (iterative-staggered) coupling method that does not use the above-mentioned fictitious fluid domain to an airbag deployment problem where a large-deformable thin structure moves in a high-speed flow field and inflation of the airbag influences

variation of the interior and exterior fluid pressures. The present method has three features. First, we use the level set function to describe complicated geometrical shapes of the fluid-structure interface on a fixed Eulerian mesh; the level set function is applicable to two-phase flow, combustion, computer graphics and more as shown in Sethian (1999), Osher and Fedkiw (2003) and Zhang *et al.* (2008). Second, we generate the level set function by using virtual nodes with level sets and structural normal velocities. The level set function represents the property of the signed distance function and can describe the large-deformable interface sufficiently. The virtual nodes are located in the direction normal to the structural mesh so as to generate the level set function on the fluid mesh and enforce the kinematic condition—that is, the continuity of normal velocities at the fluid-structure interface. Third, we solve structural variables and fluid variables separately until both converge. Our reason for adopting a partitioned-solution coupling method is that we can combine advanced fluid and structure solvers—specifically, the constrained interpolation profile finite element method (CIP-FEM) by Makihara *et al.* (1999) for the fluid and large-deformable structural elements by Dvorkin *et al.* (1988) and Noguchi and Hisada (1993) for the structure—and easily apply the method to large-scale problems.

A few studies have already applied fixed Eulerian mesh-based schemes based on the level set function to FSI problems as shown in Bungartz and Schafer (2007) and Sawada *et al.* (2009). Cirak and Radovitzky (2005) applied loose (one-way) coupling to unfolded airbag deployment. Legay *et al.* (2006) proposed a simultaneous-solution (monolithic) method where the Lagrange multiplier is introduced to impose the kinematic condition at the fluid-structure interface. The method of Legay *et al.* (2006) was applied to a slightly compressible water channel flow closed by a thin elastic structure. We also compare the present coupling method with the moving ALE mesh-based scheme of LS-DYNA and the fixed Eulerian mesh-based scheme of Legay *et al.* (2006) for applicability to finite-deformation FSI problems in this work.

This paper is structured as follows: In section 2, we state the governing equations for FSI and interface conditions. In section 3, we discuss our computational methods, in particular finite element methods for the fluid and structure, interface-treatment using the level set function generated by virtual nodes and a partitioned-solution method. In section 4, we confirm that virtual nodes are capable of generating the level set function that sufficiently represents the property of the signed distance function. In section 5, we handle finite-deformation problems, and compare the proposed method, the moving ALE mesh-based scheme, and the fixed Eulerian mesh-based scheme of Legay *et al.* (2006) for code and calculation verification. In section 6, we show that the proposed method is applicable to unfolded airbag deployment simulations. In section 7, we present concluding remarks and describe our future plans.

2. Governing equations

2.1 Structure

The structure is assumed to be compressible and elastic. The equations of motion, using a Lagrangian description, are

$${}^0\rho\frac{d^2\mathbf{u}}{dt^2} = {}^0\nabla \cdot (\mathbf{S} \cdot \mathbf{F}^T) \quad (1)$$

where d/dt is the material time derivative, ${}^0\rho$ is the initial density, ${}^0\nabla$ is the gradient operator taken with respect to the material coordinate, \mathbf{u} is the displacement, the superscript T denotes the transpose of a tensor and \mathbf{F} is the deformation gradient tensor described by the identity tensor \mathbf{I} as follows

$$\mathbf{F} = \mathbf{I} + ({}^0\nabla \otimes \mathbf{u})^T \quad (2)$$

The material is specified by giving the second Piola-Kirchhoff stress tensor \mathbf{S} according to the following constitutive law for St. Venant-Kirchhoff materials

$$\mathbf{S} = \lambda(\text{tr}\mathbf{E})\mathbf{I} + 2\mu\mathbf{E} \quad (3)$$

where \mathbf{E} is the Green-Lagrange strain tensor given by

$$\mathbf{E} = \frac{1}{2}(\mathbf{F} \cdot \mathbf{F}^T - \mathbf{I}) \quad (4)$$

The elasticity of the material is characterized by the Young's modulus E and the Poisson's ratio ν . The alternative characterization is described by the Lamé coefficients λ and μ :

$$\lambda = \frac{E\nu}{(1+\nu)(1-2\nu)} \quad (5)$$

$$\mu = \frac{E}{2(1+\nu)} \quad (6)$$

2.2 Fluid

The fluid is assumed to be a compressible, inviscid and adiabatic ideal gas. The continuity equation, equations of motion and pressure equation, using an Eulerian description, are

$$\frac{\partial \rho}{\partial t} + (\mathbf{v} \cdot \nabla)\rho = -\rho(\nabla \cdot \mathbf{v}) \quad (7)$$

$$\rho \frac{\partial \mathbf{v}}{\partial t} + \rho(\mathbf{v} \cdot \nabla)\mathbf{v} = -\nabla p \quad (8)$$

$$\frac{\partial p}{\partial t} + (\mathbf{v} \cdot \nabla)p = -\kappa p \nabla \cdot \mathbf{v} \quad (9)$$

where ρ is the density, $\partial/\partial t$ is the spatial time derivative, ∇ is the gradient operator taken with respect to the spatial coordinates, \mathbf{v} is the velocity, p is the pressure and κ is the specific heat ratio. If the fluid is slightly compressible water, instead of Eq. (9) we use the equation of state as shown in Legay *et al.* (2006)

$$p = {}^0\rho c_w^2 \left(1 - \frac{{}^0\rho}{\rho}\right) \quad (10)$$

where c_w is the sound speed of water.

In this study, it is necessary to obtain the derivatives to enable use of the CIP-FEM. We rewrite the Eqs. (7)-(9) as

$$\frac{\partial \mathbf{f}}{\partial t} + (\mathbf{v} \cdot \nabla)\mathbf{f} = \mathbf{g} \quad (11)$$

$$\frac{\partial \mathbf{f}_i}{\partial t} + (\mathbf{v} \cdot \nabla) \mathbf{f}_i + (\mathbf{v}_i \cdot \nabla) \mathbf{f} = \mathbf{g}_i \quad (12)$$

where the subscript, i denotes the derivative with respect to the x_i coordinate, and \mathbf{f} and \mathbf{g} are

$$\mathbf{f} = \begin{pmatrix} \rho \\ \mathbf{v} \\ p \end{pmatrix} \quad (13)$$

$$\mathbf{g} = \begin{pmatrix} \mathbf{g}_\rho \\ \mathbf{g}_v \\ \mathbf{g}_p \end{pmatrix} = \begin{pmatrix} -\rho \nabla \cdot \mathbf{v} \\ -\frac{\nabla p}{\rho} \\ -\kappa p \nabla \cdot \mathbf{v} \end{pmatrix} \quad (14)$$

2.3 Interface conditions

The boundary conditions at the fluid-structure interface are kinematic and dynamic coupling conditions. Because no mass flow across the interface is assumed, the normal velocities at the interface must match. The kinematic condition is

$$\mathbf{n} \cdot \mathbf{v}_f = \mathbf{n} \cdot \frac{d\mathbf{u}_s}{dt} \quad (15)$$

where \mathbf{n} is the unit vector normal to the interface, \mathbf{v}_f is the fluid velocity and \mathbf{u}_s is the structural displacement. It is necessary for the traction vectors to be equal so as to enforce equilibrium of forces at the fluid-structure interface. The dynamic conditions are

$$-p\mathbf{n} = \mathbf{n} \cdot \mathbf{T}_s \quad (16)$$

where \mathbf{T}_s is the structural Cauchy stress tensor.

3. Computational methods

3.1 Computational domains and meshes

Fig. 1 shows a schematic diagram of the computational domains and meshes. The computational domains consist of the involved physical fluid domain Ω_f , structural domain Ω_s and the void (that is, fictitious fluid) domain Ω_v . In the void domain, the Dirichlet boundary conditions for the fluid variables are applied to satisfy the kinematic condition. The computational meshes are divided into an overlapping, moving Lagrangian mesh for the structural domain and a fixed Eulerian mesh for the fluid and void domains. As a structural mesh, in 2D we use 2-node beam elements by Dvorkin *et al.* (1988) and in 3D we use 4-node shell elements by Noguchi and Hisada (1993). As a fluid mesh, in 2D we use 4-node quadrilateral elements and in 3D we use 8-node hexahedral elements for the CIP-FEM of Makihara *et al.* (1999). Because the structure is assumed to be sufficiently thin, the mid-surface of the structure corresponds to the fluid-structure interface Γ_i . The geometrical shapes of the deformable mid-surface are represented as a zero isosurface of the level set function

$${}^{n+1}\left(\frac{d\mathbf{u}}{dt}\right) = {}^n\left(\frac{d\mathbf{u}}{dt}\right) + \Delta t \left\{ \gamma {}^{n+1}\left(\frac{d^2\mathbf{u}}{dt^2}\right) + (1-\gamma) {}^n\left(\frac{d^2\mathbf{u}}{dt^2}\right) \right\} \quad (18)$$

$${}^{n+1}\mathbf{u} = {}^n\mathbf{u} + \Delta t {}^n\left(\frac{d\mathbf{u}}{dt}\right) + \Delta t^2 \left\{ \beta {}^{n+1}\left(\frac{d^2\mathbf{u}}{dt^2}\right) + \left(\frac{1}{2} - \beta\right) {}^n\left(\frac{d^2\mathbf{u}}{dt^2}\right) \right\} \quad (19)$$

where γ and β are the Newmark's parameters; in this study, $\gamma = 0.5$ and $\beta = 0.25$. For a linear system, the choice of $\gamma = 0.5$ and $\beta = 0.25$ can produce an unconditionally stable system. Multiplying Eq. (1) by any arbitrary weight function $\delta\mathbf{u}$ and integrating over the structural domain ${}^0\Omega_s$ gives the weak form

$$\int_{{}^0\Omega_s} \delta\mathbf{u} \cdot {}^0\rho \frac{d^2\mathbf{u}}{dt^2} d^0\Omega = \int_{{}^0\Omega_s} \delta\mathbf{u} \cdot \mathbf{t} d\Gamma - \int_{{}^0\Omega_s} (\nabla \otimes \delta\mathbf{u}) : (\mathbf{S} \cdot \mathbf{F}^T) d^0\Omega \quad (20)$$

We discretize the governing equations for the structure by the structural elements, and calculate the displacement, velocity and acceleration at each node.

3.3 Fluid

We can discretize the governing equations, i.e., Eqs. (11) and (12), by applying a semi-Lagrangian method, then divide them into its advection and non-advection phases written as

$$\hat{\mathbf{f}}(\mathbf{x}) = {}^n\mathbf{f}(\mathbf{x} - {}^n\mathbf{v}(\mathbf{x})\Delta t) \quad (21)$$

$$\hat{\mathbf{f}}_{,i}(\mathbf{x}) = {}^n\mathbf{f}_{,i}(\mathbf{x} - {}^n\mathbf{v}(\mathbf{x})\Delta t) - \Delta t \sum_j \frac{\partial^n v_j}{\partial x_i} {}^n\mathbf{f}_{,j}(\mathbf{x} - {}^n\mathbf{v}(\mathbf{x})\Delta t) \quad (22)$$

$$\frac{{}^{n+1}\mathbf{f} - \hat{\mathbf{f}}}{\Delta t} = \gamma {}^{n+1}\mathbf{g}' + (1-\gamma) {}^n\mathbf{g}' \quad (23)$$

$$\frac{{}^{n+1}\mathbf{f}_{,i} - \hat{\mathbf{f}}_{,i}}{\Delta t} = \gamma {}^{n+1}\mathbf{g}'_{,i} + (1-\gamma) {}^n\mathbf{g}'_{,i} \quad (24)$$

where \mathbf{g}' is

$$\mathbf{g}' = \begin{pmatrix} g'_\rho \\ \mathbf{g}'_v \\ g'_p \end{pmatrix} = \begin{pmatrix} -\rho \nabla \cdot \mathbf{v} \\ -\frac{\nabla(p+q)}{\rho} \\ -\{\kappa p + (\kappa-1)q\} \nabla \cdot \mathbf{v} \end{pmatrix} \quad (25)$$

and γ is the Crank-Nicolson parameter; in this study, $\gamma = 0.5$. The choice of $\gamma = 0.5$ can produce a second-order time-marching scheme. The von Neumann-Richtmyer type artificial viscosity by von Neumann and Richtmyer (1950) and Wilkins (1980) is defined as

$$q = \begin{cases} \rho(\alpha_q c |\nabla \cdot \mathbf{v}| \Delta L + \beta_q |\nabla \cdot \mathbf{v}|^2 \Delta L^2) & (\nabla \cdot \mathbf{v} < 0) \\ 0 & (\nabla \cdot \mathbf{v} \geq 0) \end{cases} \quad (26)$$

where α_q and β_q are the parameters, ΔL is the grid size and c is the sound speed. If the fluid is assumed to be an ideal gas, the sound speed is

$$c = \sqrt{\frac{\kappa \mathcal{P}}{\rho}} \quad (27)$$

The CIP method by Takewaki *et al.* (1985) is well-known as the effective finite difference scheme for solving the advection equation, and the CIP-FEM by Makihara *et al.* (1999) is the CIP method applicable to an unstructured grid. We solve Eqs. (21) and (22) using the CIP-FEM, and obtain \mathbf{f} and \mathbf{f}_i . The CIP-FEM uses a conventional linear mapping function and a cubic interpolation function that satisfies the continuity of a function and the derivative at each fluid node. The use of finite elements makes it possible to describe complicated geometry. The order of the interpolation function is lowered so that numerical oscillation does not arise near a shock wave. We solve Eqs. (23) and (24) and obtain ${}^{n+1}\mathbf{f}$ and ${}^{n+1}\mathbf{f}_i$. Multiplying Eq. (25) by any arbitrary weight function $\delta\rho$, $\delta\mathbf{v}$ or δp and the approximate Heaviside function $H_\varepsilon(\phi)$ and integrating over the fluid and void domains $\Omega_\pm = \Omega_+ \cup \Omega_-$ gives the weak forms

$$\int_{\Omega_\pm} \delta\rho g_\rho H_\varepsilon(\phi) d\Omega = - \int_{\Omega_\pm} \delta\rho (\rho \nabla \cdot \mathbf{v}) H_\varepsilon(\phi) d\Omega \quad (28)$$

$$\begin{aligned} \int_{\Omega_\pm} \delta\mathbf{v} \cdot \mathbf{g}_v H_\varepsilon(\phi) d\Omega &= \int_{\partial\Omega_\pm} \delta\mathbf{v} \cdot (-p\mathbf{n}) H_\varepsilon(\phi) d\Gamma \\ &+ \int_{\Omega_\pm} (\nabla \cdot \delta\mathbf{v})(p+q) H_\varepsilon(\phi) d\Omega \\ &- \int_{\Omega_\pm} \delta\mathbf{v} \cdot \{(p+q)\mathbf{n}_\phi\} \delta_\varepsilon(\phi) |\nabla\phi| d\Omega \end{aligned} \quad (29)$$

$$\int_{\Omega_\pm} \delta p g_p H_\varepsilon(\phi) d\Omega = - \int_{\Omega_\pm} \delta p [\{\kappa p + (\kappa-1)q\} \nabla \cdot \mathbf{v}] H_\varepsilon(\phi) d\Omega \quad (30)$$

where $q = 0$ on $\partial\Omega_\pm$ and the unit vector normal to the isosurface of the level set function \mathbf{n}_ϕ is defined as

$$\mathbf{n}_\phi = -\frac{\nabla\phi}{|\nabla\phi|} \quad (31)$$

The approximate Heaviside function $H_\varepsilon(\phi)$ and the approximate delta function $\delta_\varepsilon(\phi)$ are defined as

$$H_\varepsilon(\phi) = \begin{cases} 1 & (\phi \geq \varepsilon) \\ \frac{1}{2} \left\{ 1 + \frac{\phi}{\varepsilon} + \frac{1}{\pi} \sin\left(\frac{\pi\phi}{\varepsilon}\right) \right\} & (|\phi| < \varepsilon) \\ 0 & (\phi \leq -\varepsilon) \end{cases} \quad (32)$$

$$\delta_\varepsilon(\phi) = \frac{dH_\varepsilon(\phi)}{d\phi} = \begin{cases} \frac{1}{2\varepsilon} \left\{ 1 + \cos\left(\frac{\pi\phi}{\varepsilon}\right) \right\} & (|\phi| < \varepsilon) \\ 0 & (|\phi| \geq \varepsilon) \end{cases} \quad (33)$$

where ε is the smoothing parameter. We can calculate delta function easily by using the approximate Heaviside function and expect smoothing effect for suppressing the instability that occurs due to discontinuity on the interface as described in Sussman *et al.* (1994). In this study, ε is three times the size of a minimum fluid node distance near the interface. If ε is too small, the solution can yield unwanted instabilities at the interface. We discretize the governing equations for the fluid by the finite elements, and calculate the density, velocity and pressure at each node.

3.4 Interface-treatment technique using the level set function generated by virtual nodes

An interface-treatment technique involves two processes: (1) generation of the level set function on the fluid mesh by using virtual nodes as the geometry of the structure deforms and (2) application of the Dirichlet boundary conditions for the fluid variables to satisfy the kinematic condition at the fluid-structure interface.

Fig. 2, upper figure shows the algorithm of the first process, which is summarized as follows:

(L1) Put virtual nodes at structural nodes \mathbf{x}_s^I . If the extension rate and curvature of the structural mesh increase due to deformation, add virtual nodes on the mid-surface of the structure at positions other than the structural nodes as follows:

(S1) Compute the distances between vertices $|\mathbf{x}_s^I - \mathbf{x}_s^J|$ and inner products $\mathbf{n}_s^I \cdot \mathbf{n}_s^J$ of unit normal vectors at vertices in a structural element.

(S2) Compute the 1D deformation gradient $s_{\text{dict}} = \text{INTEGER}(|\mathbf{x}_s^I - \mathbf{x}_s^J| / |\mathbf{x}_s^I - \mathbf{x}_s^J|)$.

(S3) Compute the angle $\theta = \cos^{-1}(\mathbf{n}_s^I \cdot \mathbf{n}_s^J)$ and obtain $s_{\text{ang}}(1, 2, \dots, \text{or } 6)$ by $(s_{\text{ang}} - 1)\pi/6 \leq \theta \leq s_{\text{ang}}\pi/6$.

(S4) Compute $s_{\text{max}} = \text{MAX}(s_{\text{dict}}, s_{\text{ang}})$.

(S5) Add virtual nodes ($(s_{\text{max}} - 1)$ nodes in 2D; $(s_{\text{max}} - 1)^2$ nodes in 3D) on the mid-surface of the structure (Fig. 3).

(L2) Arrange virtual nodes at regular intervals of the minimal structural node distance 0L_s in the direction normal to the interface from each virtual node that has already been added.

(L3) Provide virtual nodes \mathbf{x}_{vp}^J with level sets $\phi_{\text{vp}}^J = 0, \pm {}^0L_s, \pm 2{}^0L_s, \pm 3{}^0L_s, \dots$ and velocities equal to the structural velocities connected by normal lines (Fig. 2, dotted lines).

(L4) Detect some virtual nodes $\mathbf{x}_{\text{nvp}}^J$ (5 nodes in 2D; 21 nodes in 3D) near fluid node \mathbf{x}^I from all the virtual nodes located on the mid-surface of the structure. Normal vectors $\mathbf{n}_{\text{nvp}}^J$ and \mathbf{n}^I at the positions of the detected virtual nodes and the fluid node must satisfy the condition $\mathbf{n}_{\text{nvp}}^J \cdot \mathbf{n}^I > 0$. Make group G_{vp}^I from the detected virtual nodes and virtual nodes connected by normal lines (Fig. 2, dotted lines).

(L5) Generate level set ϕ^I at fluid node \mathbf{x}^I near the interface using the moving least squares (MLS) approximation $\phi^I \approx \phi_{\text{MLS}}(\mathbf{x}^I)$ (see Lancaster and Salkauskas 1981) from the sampling data of level sets ϕ_{vp}^J of virtual nodes \mathbf{x}_{vp}^J in group G_{vp}^I . The radius of the influence domain proportionally changes according to the distance between virtual nodes on the mid-surface of the structure so as to provide sufficient accuracy for the MLS approximation. In the MLS

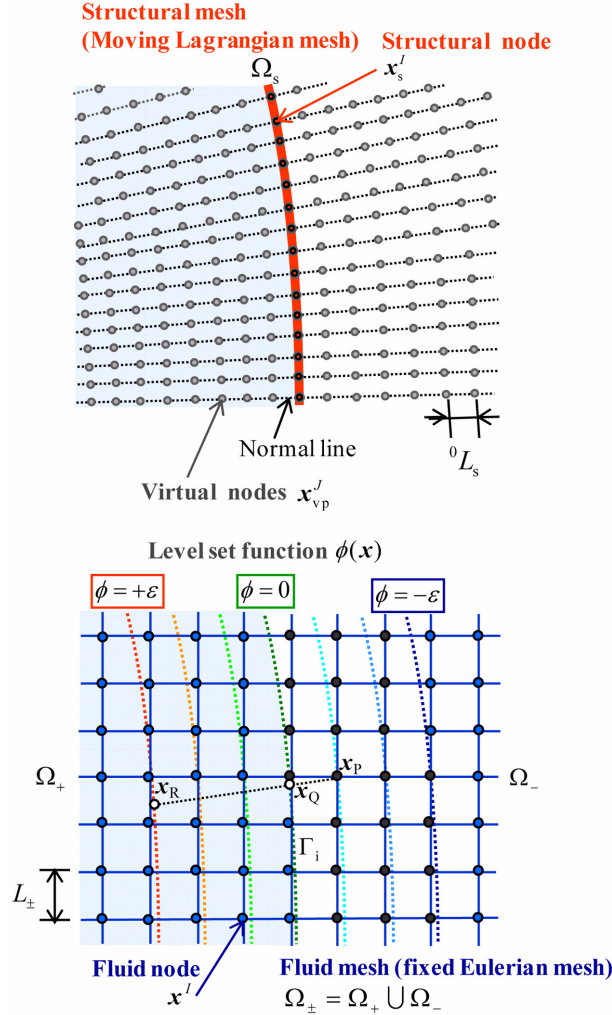


Fig. 2 Interface-treatment method using virtual nodes: generation of the level-set function (upper figure) and application of the Dirichlet boundary conditions (lower figure)

approximation, the weight function is the cubic spline function, and the polynomial basis vector is linear as shown in Hashimoto and Noguchi (2008). The x_i component of the gradient of the level set function $(\nabla \phi)^I$ is easily obtained by $(\nabla \phi)^I \simeq (\nabla \phi_{MLS}) \Big|_{x=x^I}$. The level set function obtained here

satisfies the property of the signed distance function $|\nabla \phi| = 1$.

Fig. 2, lower figure shows the algorithm of the second process, which is summarized as follows:

(D1) Define fluid node x^I in the range $-\varepsilon \leq \phi^I < 0$ as point x_p . The Dirichlet boundary conditions for the fluid variables are given at point x_p .

(D2) Define points x_Q and x_R in direction $(\nabla \phi)_p / |(\nabla \phi)_p|$ at point x_p . The separation distance is $|\phi_p|$ from point x_p to point x_Q , and ε from point x_Q to point x_R .

(D3) Obtain fluid variables $\mathbf{f}_R = (\rho_R, \mathbf{v}_R, p_R)^T$ at point x_R using the MLS approximations

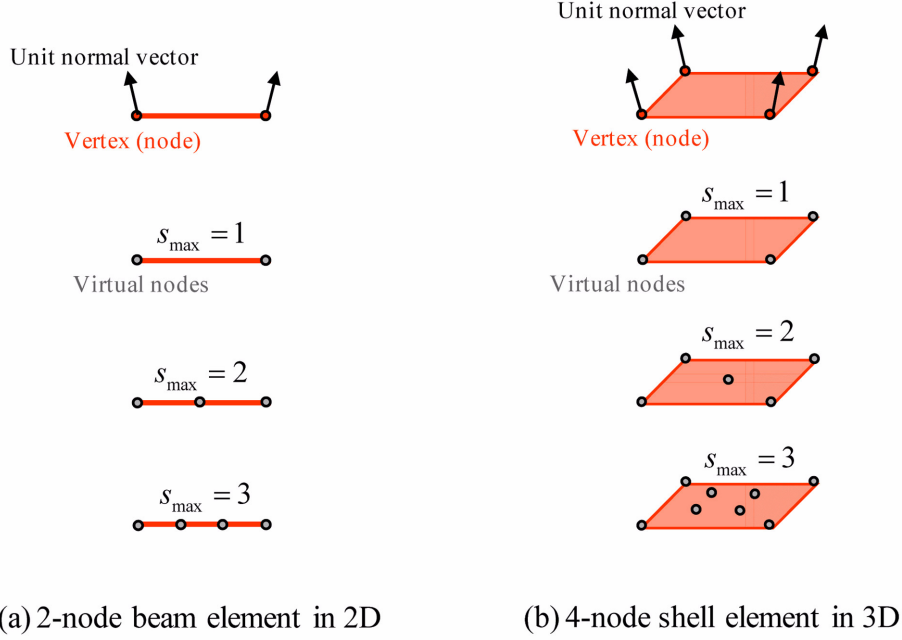


Fig. 3 Positions of virtual nodes on beam and shell elements

$\rho_R \approx \rho_{MLS}(\mathbf{x}_R)$, $\mathbf{v}_R \approx \mathbf{v}_{MLS}(\mathbf{x}_R)$, and $p_R \approx p_{MLS}(\mathbf{x}_R)$ from the sampling data of fluid variables $\mathbf{f}^j = (\rho^j, \mathbf{v}^j, p^j)^T$ of fluid nodes \mathbf{x}^j . Obtain fluid variables $\mathbf{f}_Q = (\rho_Q, \mathbf{v}_Q, p_Q)^T$ at point \mathbf{x}_Q by decomposing \mathbf{v}_Q into the normal velocity $(v_n)_Q$ and tangent velocity $(v_t)_Q$ as $\mathbf{v}_Q = (v_n)_Q \mathbf{n}_Q + (v_t)_Q \mathbf{t}_Q$ and using the MLS approximation $(v_n)_Q \approx (v_n)_{MLS}(\mathbf{x}_Q)$ from the sampling data of normal velocities $(v_n)_{vp}^j$ of virtual nodes \mathbf{x}_{vp}^j and the MLS approximations $\rho_Q \approx \rho_{MLS}(\mathbf{x}_Q)$, $(v_t)_Q \approx (v_t)_{MLS}(\mathbf{x}_Q)$, and $p_Q \approx p_{MLS}(\mathbf{x}_Q)$ from the sampling data of densities ρ^j , tangent velocities $(v_t)^j$, and pressures p^j of fluid nodes \mathbf{x}^j .

(D4) Obtain fluid variables \mathbf{f}_p at point \mathbf{x}_p by extrapolation as

$$\mathbf{f}_p = \left(1 - \frac{\phi_p}{\phi_R}\right) \mathbf{f}_Q + \frac{\phi_p}{\phi_R} \mathbf{f}_R \quad (34)$$

Enright *et al.* (2002) proposed a hybrid particle level set method where the level set function is used to represent the interface that changes in a flow field. The particles used in the Enright method have level sets like the level-set virtual nodes of the present coupling method. However, they differ in that they are irregularly scattered near the interface and move as marker particles by the Lagrange method. When the marker particles cross the interface, level-set loss is modified so as to obtain the zero level set accurately. However, because the level set function does not sufficiently satisfy the property of the signed distance function obtained by the hybrid particle level set method, it is necessary to compute reinitialization as shown in Osher and Fedkiw (2003).

3.5 Partitioned-solution coupling method

This coupling is formulated as a Block Gauss-Seidel iterative scheme accelerated by the Aitken

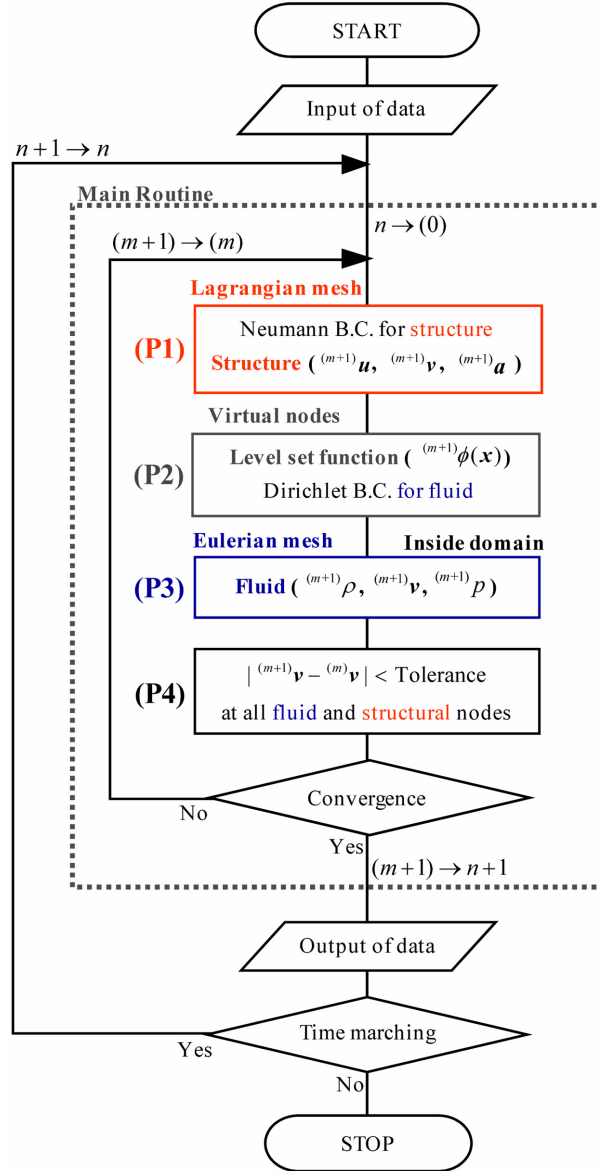


Fig. 4 Partitioned-solution coupling method (n : time step; m): iteration)

method as shown in Joosten *et al.* (2009). Fig. 4 shows the algorithm of the partitioned-solution coupling method, which is summarized as follows:

(P1) Obtain the traction

$$\mathbf{n} \cdot \mathbf{T}_s = -p\mathbf{n} \tag{35}$$

as the Neumann boundary conditions for the structural variables by interpolating from the fluid pressures $p(\mathbf{x}_s^f)$ at structural nodes \mathbf{x}_s^f . The fluid pressures at the structural nodes are

$$p(\mathbf{x}_s^I) = \begin{cases} p_{\text{MLS}}(\mathbf{x}_s^I) & \text{on the fluid domain side} \\ p_v & \text{on the void domain side} \end{cases} \quad (36)$$

where $p_{\text{MLS}}(\mathbf{x}_s^I)$ denotes the MLS approximation from the sampling data of fluid pressure p^J , and p_v is the pressure in the void domain. Compute the structural displacement \mathbf{u} , velocity \mathbf{v} and acceleration \mathbf{a} . The structural normal velocity ${}^{(m+1)}\mathbf{v}_n$ at Block Gauss-Seidel iteration $(m+1)$ is computed as

$${}^{(m+1)}\mathbf{v}_n = {}^{(m)}\omega {}^{(m+1)}\tilde{\mathbf{v}}_n + (1 - {}^{(m)}\omega) {}^{(m)}\mathbf{v}_n \quad (37)$$

where ${}^{(m+1)}\tilde{\mathbf{v}}_n$ is the column vector composed of the structural normal velocity at the interface and ${}^{(m)}\omega = 1 - {}^{(m)}\mu$ is the relaxation parameter. The Aitken factor ${}^{(m)}\mu$ is obtained from

$$\mu^{(m)} = \mu^{(m-1)} + (\mu^{(m-1)} - 1) \frac{({}^{(m-1)}\Delta\mathbf{v}_n - {}^{(m)}\Delta\mathbf{v}_n)^T ({}^{(m)}\Delta\mathbf{v}_n)}{({}^{(m-1)}\Delta\mathbf{v}_n - {}^{(m)}\Delta\mathbf{v}_n)^T ({}^{(m-1)}\Delta\mathbf{v}_n - {}^{(m)}\Delta\mathbf{v}_n)} \quad (38)$$

where the interfacial normal velocity difference ${}^{(m)}\Delta\mathbf{v}_n$ is computed as

$${}^{(m)}\Delta\mathbf{v}_n = {}^{(m-1)}\mathbf{v}_n - {}^{(m)}\tilde{\mathbf{v}}_n \quad (39)$$

(P2) Generate the level set function $\phi(\mathbf{x})$ on the fluid mesh and apply the Dirichlet boundary conditions for the fluid variables in the void domain using the level set function generated by virtual nodes.

(P3) Compute the fluid density ρ , velocity \mathbf{v} and pressure p .

(P4) If the velocities at all fluid and structural nodes converge, proceed to the next time step.

3.6 Coupling procedure for fluid domains divided by thin elastic structure

We handle the fluid domains on both sides of the structure (Fig. 5, upper figure) so that we can predict pressure variation on the outside. Computation for the fluid domains is separated into interior and exterior fluid steps (Fig. 5, lower figures). To obtain the fluid variables on the inside of the structure, we follow the above-mentioned coupling method. To obtain the fluid variables on the outside of the structure, we reverse the sign of the level set function that has been already obtained ($-\phi(\mathbf{x}) \rightarrow \phi(\mathbf{x})$) and the Dirichlet boundary conditions for the exterior fluid variables are provided in the interior void domain. As shown in Fig. 6, two steps (P2)' and (P3)' are added to the coupling method in Fig. 4. The algorithm of the partitioned-solution coupling method is summarized as follows:

(P1) Obtain the traction as the Neumann boundary conditions for the structural variables by interpolating from the fluid pressures $p(\mathbf{x}_s^I)$ at structural nodes \mathbf{x}_s^I . The fluid pressures at the structural nodes are

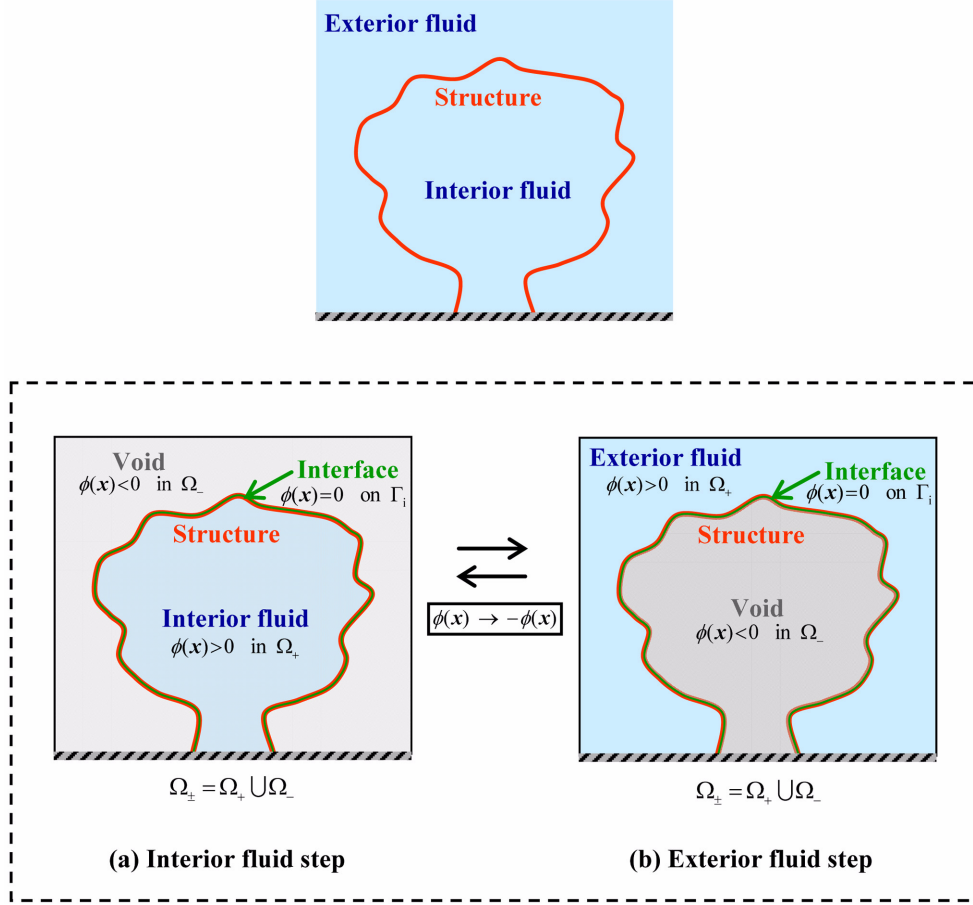


Fig. 5 Computational domains

$$p(\mathbf{x}_s^I) = \begin{cases} (p_{\text{in}})_{\text{MLS}}(\mathbf{x}_s^I) & \text{on the interior fluid domain side} \\ (p_{\text{ex}})_{\text{MLS}}(\mathbf{x}_s^I) & \text{on the exterior fluid domain side} \end{cases} \quad (40)$$

where $(p_{\text{in}})_{\text{MLS}}(\mathbf{x}_s^I)$ and $(p_{\text{ex}})_{\text{MLS}}(\mathbf{x}_s^I)$ denote the MLS approximations from the sampling data of interior and exterior fluid pressures p^I respectively. Compute the structural displacement \mathbf{u} , velocity \mathbf{v} and acceleration \mathbf{a} . Following the Aitken method, the structural normal velocity at is computed in the same way of Eqs. (37)-(39).

(P2) Generate the level set function $\phi(\mathbf{x})$ on the fluid mesh and apply the Dirichlet boundary conditions for the interior fluid variables in the exterior void domain using the level set function generated by virtual nodes.

(P3) Compute the interior fluid density ρ , velocity \mathbf{v} and pressure p .

(P2)' Reverse the sign of the level set function $-\phi(\mathbf{x}) \rightarrow \phi(\mathbf{x})$ on the fluid mesh and apply the Dirichlet boundary conditions for the exterior fluid variables in the interior void domain using the

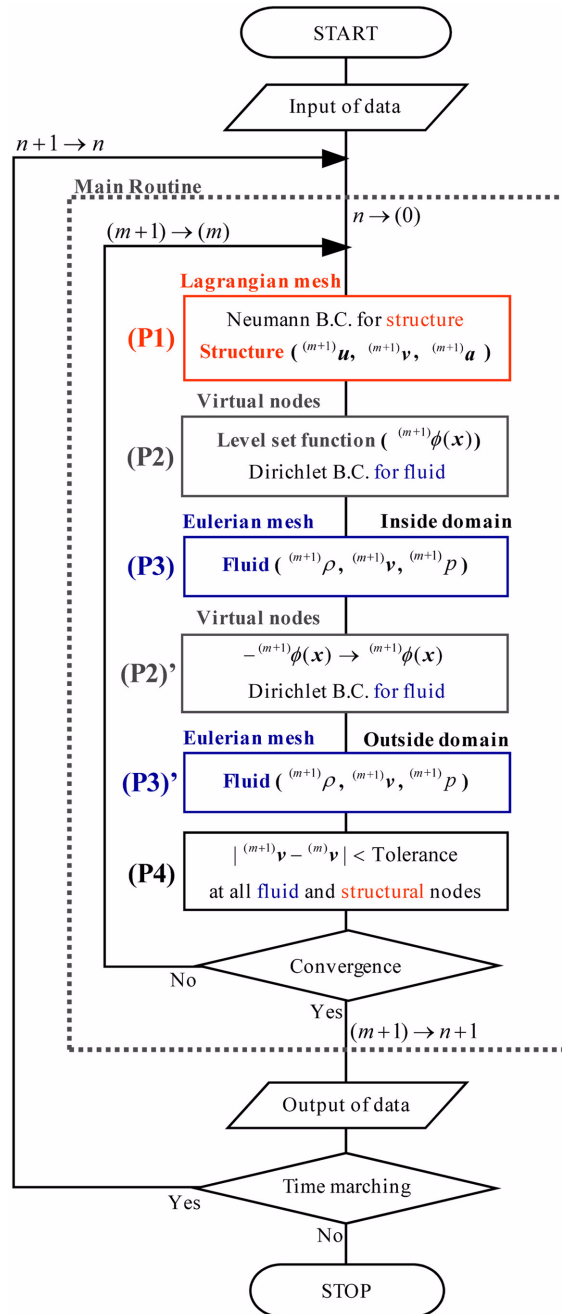


Fig. 6 Partitioned-solution coupling method (n : time step; m): iteration)

level set function generated by virtual nodes.

(P3)' Compute the exterior fluid density ρ , velocity \mathbf{v} and pressure p .

(P4) If the velocities at all fluid and structural nodes converge, proceed to the next time step.

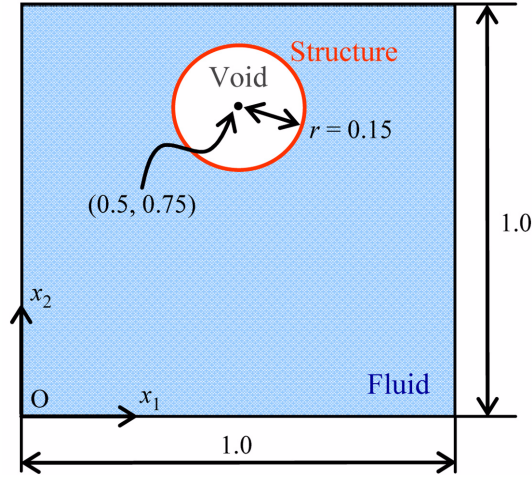


Fig. 7 2D analysis model of a vortex in a box

4. Generation of level set function

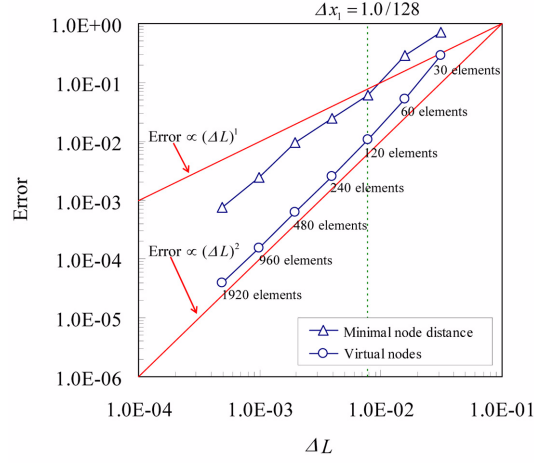
It is important to satisfy the kinematic condition at the interface. The accuracy of the FSI solution depends on the extrapolation of Eq. (34). The extrapolation is derived using the properties of the signed distance function, $|\nabla\phi| = 1$. The accuracy of $|\nabla\phi| = 1$ is associated with adequacy of boundary conditions for fluid. In this section, it is confirmed that virtual nodes are capable of generating the level set function that sufficiently represents $|\nabla\phi| = 1$. Fig. 7 shows a 2D model of a vortex in a box. The fluid mesh has rectangular 4-node quadrilateral elements of 128×128 divisions (element size: $\Delta x_1 = \Delta x_2 = 7.8125 \times 10^{-3}$); the structural mesh has 2-node line elements of 480 divisions (element size: $\Delta L = 1.9635 \times 10^{-3}$). Because the structural mesh deforms according to a velocity distribution, this problem is not a FSI problem. The level set function is generated near the interface ($|\phi(\mathbf{x})| < 3\Delta x_1$) on the fixed Eulerian mesh. The structural velocity components are

$$v_1 = -\sin^2(\pi x_1) \sin(2\pi x_2) \quad (41)$$

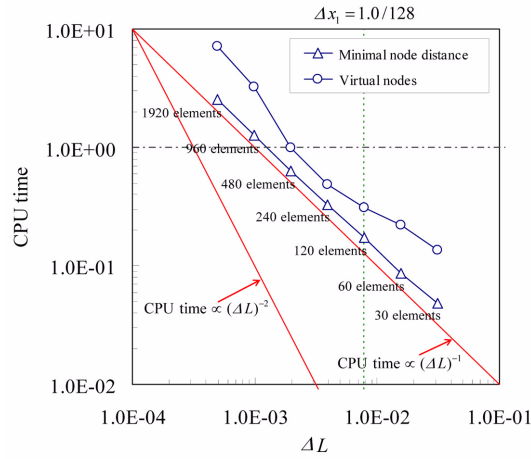
$$v_2 = \sin(2\pi x_1) \sin^2(\pi x_2) \quad (42)$$

We first investigate the CPU time required for generation of the level set function and the error for $|\phi(\mathbf{x})| < \Delta x_1$ at $t = 0.0$. In this study, we call the method for obtaining the level set function from the distance and direction vector from a fluid node to the nearest structural node the “minimal node distance” method. The interface-treatment method using virtual nodes and the minimal node distance method are compared. The error in subdomain $\Lambda \equiv \{\mathbf{x} \mid |\phi(\mathbf{x})| \leq \Delta x_1\}$ is defined as

$$\text{Error} = \frac{1}{\Delta x_1} \frac{\sum_{l \in \Lambda} |\phi^l - \phi_{\text{exact}}(\mathbf{x}^l)|}{N_\Lambda} \quad (43)$$



(a) Error



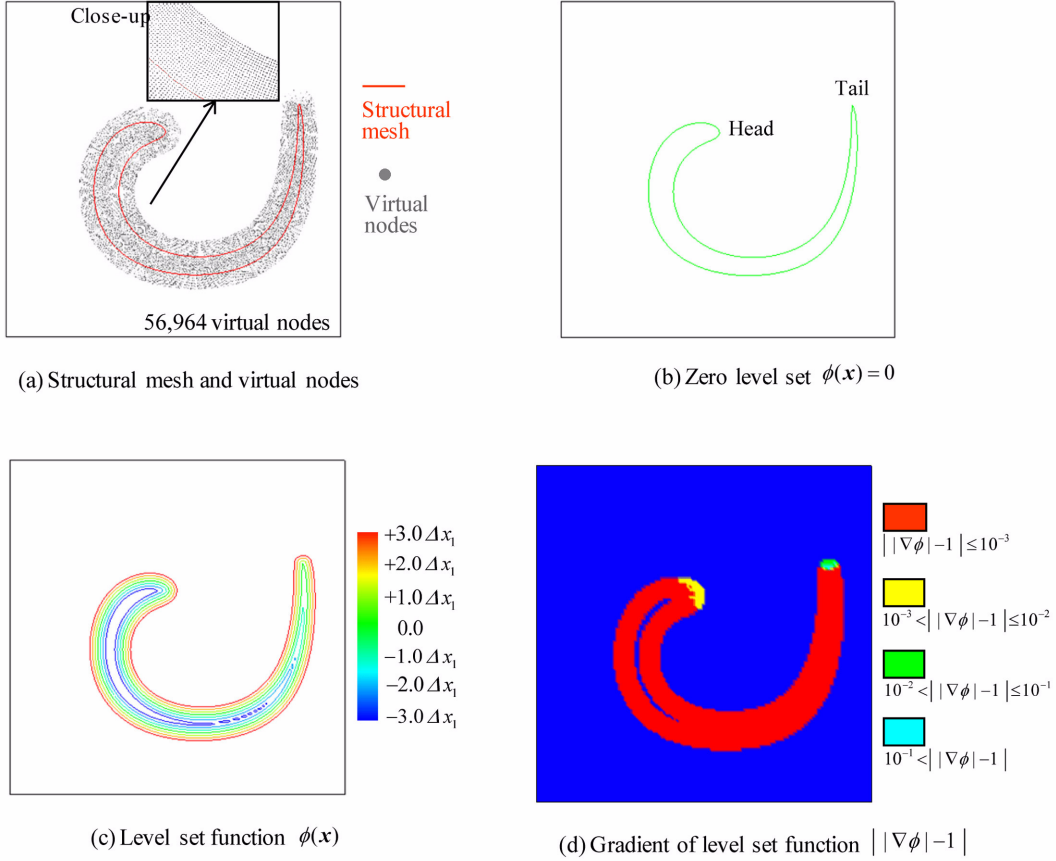
(b) CPU time

Fig. 8 Comparisons of minimal node distance method and interface-treatment method using virtual nodes

$$\phi_{\text{exact}}(\mathbf{x}) = r(\mathbf{x}) - 0.15 \quad (44)$$

$$r(\mathbf{x}) = \sqrt{(x_1 - 0.15)^2 + (x_2 - 0.75)^2} \quad (45)$$

where N_Λ is the number of fluid nodes in subdomain Λ . Fig. 8 shows CPU times and errors for the following numbers of structural elements: 30, 60, 120, 240, 480, 960 and 1920. Although the accuracy of the approximate solutions obtained for the number of structural elements 480 by using the interface-treatment method is almost the same as that obtained for the number of structural elements 1920 by using the minimal node distance method, the former method requires less CPU time.

Fig. 9 Generation of level set function on fluid mesh at $t = 1.0$

We next generate the level set function at $t = 1.0$ and $t = 3.0$ (Figs. 9 and 10) using the interface-treatment method and verify the absolute value of the gradient $|\nabla\phi|$ at fluid node \mathbf{x}^j . The structural mesh is moved by the fourth-order Runge-Kutta (RK4) method with time increment $\Delta t = 1.0 \times 10^{-2}$. $|\nabla\phi| - 1$ is mostly less than the order of 10^{-3} near the interface and less than 10^{-1} near the head of the structure except for the tail of the structural mesh. Therefore, the interface-treatment method can generate the level set function that represents the property of the signed distance function $|\nabla\phi| = 1$.

5. Finite-deformation FSI problems

5.1 Coupled analysis of a water/spring-piston system

Fig. 11 shows a 2D analysis model of a water/spring-piston system, as well as the boundary conditions. The model is a water channel closed by a spring-piston system. A slip condition is applied on the top and bottom boundaries and an incident pressure is applied on the left boundary.

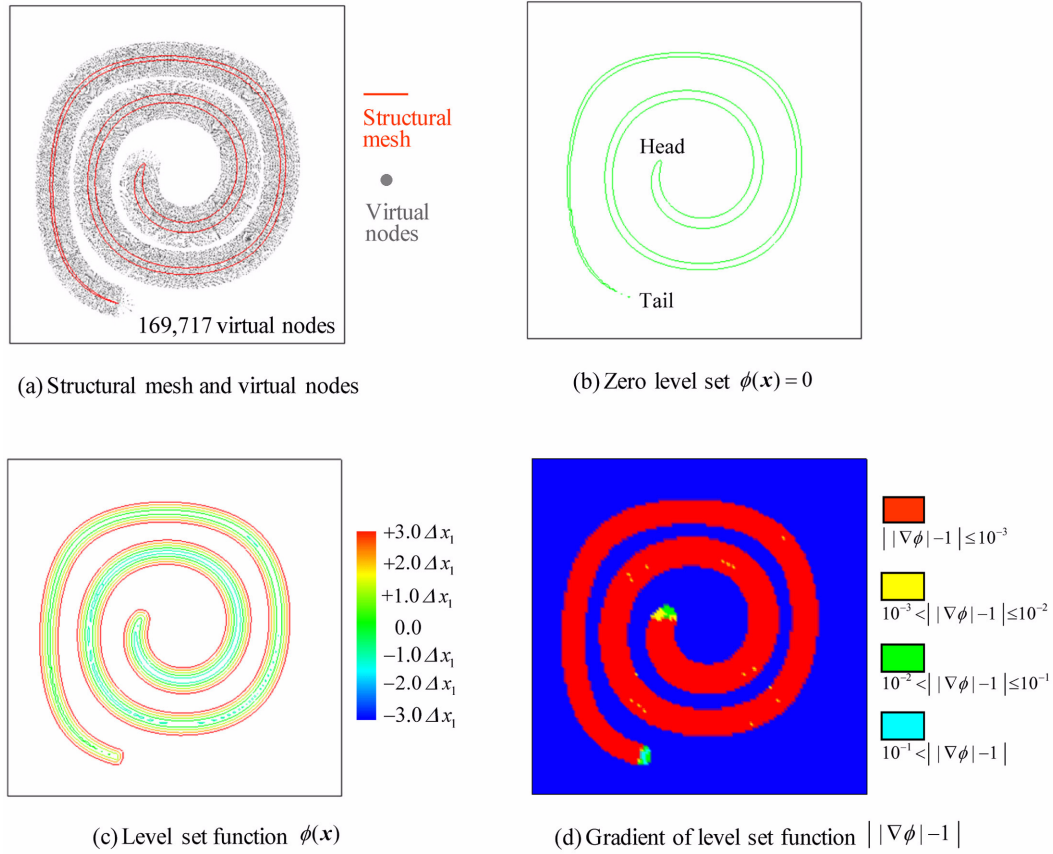


Fig. 10 Generation of level set function on fluid mesh at $t = 3.0$

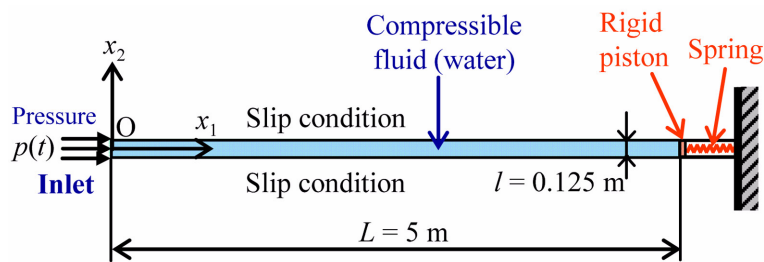


Fig. 11 2D analysis model of a water/spring-piston system

We use a 1D spring-piston system governed by the equations of motion

$$M \frac{du_1}{dt} + Ku_1 = p(x_s)l \quad (46)$$

where M is the mass, K is the spring coefficient and $p(x_s)$ is the fluid pressure acting on the piston. The incident pressure on the left boundary has the following time history

Table 1 Parameters for water (water/piston-spring system)

Symbol	Meaning	Value
${}^0\rho$	Initial density	$1.0 \times 10^3 \text{ kg/m}^3$
c_w	Sound speed	1,445 m/s
p_A	Pressure parameter	$21.0 \times 10^6 \text{ Pa}$
t_A	Time parameter	$1.4 \times 10^{-3} \text{ s}$
t_B	Time parameter	$2.8 \times 10^{-3} \text{ s}$

Table 2 Parameters for spring-piston system (water/spring-piston system)

Symbol	Meaning	Value
ρ	Density	$7.8 \times 10^3 \text{ kg/m}^3$
a	Thickness	$2.5 \times 10^{-2} \text{ m}$
K	Spring coefficient	$5.25 \times 10^7 \text{ N/m}$

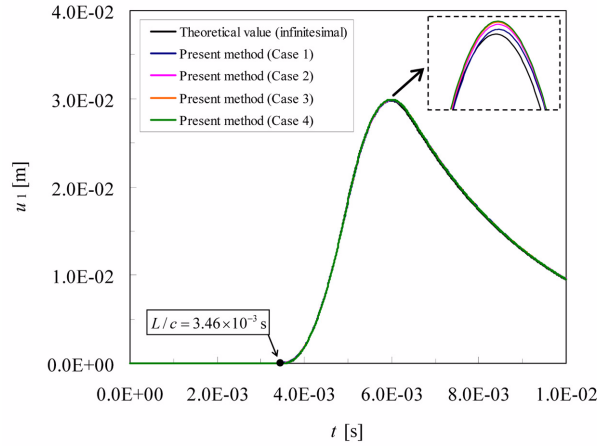
Table 3 Calculation conditions (water/spring-piston system)

	Fluid element	Structural element	Time increment Δt
Case 1	176×4	4	$2.0 \times 10^{-6} \text{ s}$
Case 2	352×8	8	$1.0 \times 10^{-6} \text{ s}$
Case 3	704×16	16	$5.0 \times 10^{-7} \text{ s}$
Case 4	1408×32	32	$2.5 \times 10^{-7} \text{ s}$

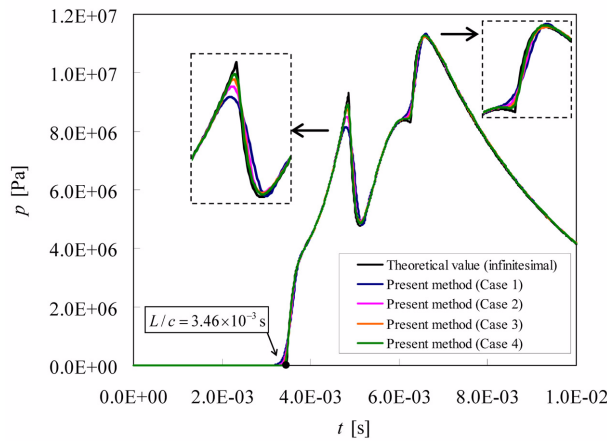
$$p = \begin{cases} p_A \left(\frac{t}{t_A} \right) & (t < t_A) \\ p_A \left(1 - \frac{t - t_A}{t_B - t_A} \right) & (t_A \leq t < t_B) \\ 0 & (t_B < t) \end{cases} \quad (47)$$

Tables 1 and 2 show the parameters for the slightly compressible inviscid water and the thin elastic structure that appear in these problems. From the tables, the arrival time of the acoustic wave is $L/c_w = 3.46 \times 10^{-3} \text{ s}$ and the mass is $M = \rho la = 24.4 \text{ kg/m}$. The void pressure is $p_v = 0.0$ and the artificial viscosity is $q = 0.0$ respectively. The fluid mesh has rectangular 4-node quadrilateral elements; the structural mesh has 2-node line elements. Connectivity of the structural nodes is not necessary for computation. Table 3 shows the numbers of elements and time increments for four cases in this study.

Fig. 12 shows time histories of the axial (u_1) displacement of the rigid piston and pressure acting on the fluid-piston interface and, for comparison, the theoretical solution obtained by infinitesimal deformation theory. The results are in good agreement with the theoretical solution. Because the fluid domain changes finitely in this analysis, the asymptotic solution of convergence does not quite correspond to the theoretical solution. The approximate solutions converge on values near the theoretical solution when the number of elements changes from Case 1 to Case 4.



(a) u_1 displacement



(b) Pressure

Fig. 12 Time histories of u_1 displacement and pressure for the water/spring-piston system

Fig. 13 shows the pressure contours on the fluid mesh for Case 4, and Fig. 14 shows the velocity distribution with isolines of the level set function ($|\phi(\mathbf{x})| \leq \varepsilon$) near the interface for Case 4. After the acoustic wave propagates in the axial direction and arrives at the fluid-piston interface, the piston is pushed in the axial direction and flow forms in the opposite direction because of the restoring force.

5.2 Coupled analysis of a water/thin-elastic-structure system

Fig. 15 shows a 2D analysis model of a water/thin-elastic-structure system, as well as the boundary conditions. This water channel is closed by a thin elastic structure. A slip condition is applied on the top boundary, a symmetric condition is applied on the bottom boundary, and the

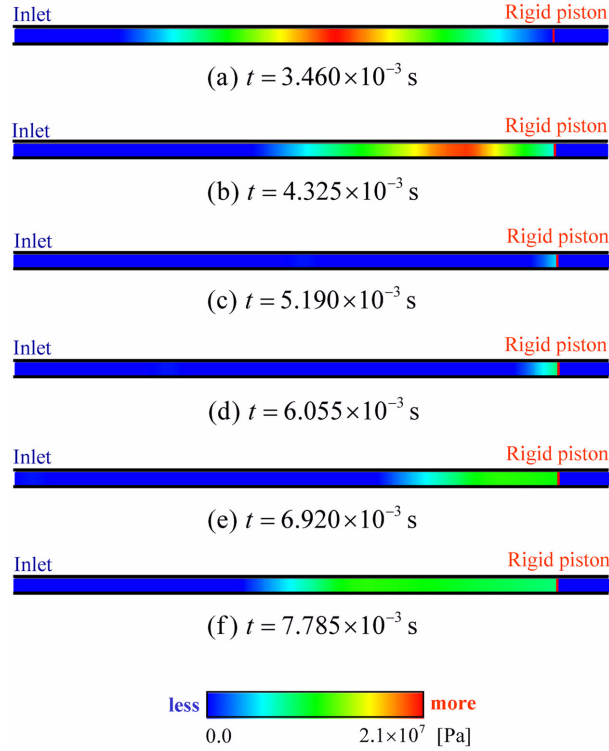


Fig. 13 Pressure contours for the water/spring-piston system

Table 4 Parameters for elastic structure (water/thin-elastic-structure system)

Symbol	Meaning	Value
ρ	Initial density	$7.8 \times 10^3 \text{ kg/m}^3$
a	Thickness	$2.5 \times 10^{-2} \text{ m}$
E	Young's modulus	$2.1 \times 10^{11} \text{ Pa}$
ν	Poisson's ratio	0.0

Table 5 Calculation conditions (water/thin-elastic-structure system)

	Fluid element	Structural element	Time increment Δt
Case 1	220×20	20	$2.5 \times 10^{-6} \text{ s}$
Case 2	440×40	40	$1.25 \times 10^{-6} \text{ s}$
Case 3	880×80	80	$6.25 \times 10^{-7} \text{ s}$

incident pressure is applied on the left boundary. The parameters in Table 1 are used for water; the incident pressure is given in Eq. (47). Table 4 shows the parameters for the thin elastic structure that appears in this problem. From Table 1, the arrival time of the acoustic wave is $L / c_w = 6.92 \times 10^{-3} \text{ s}$. The void pressure is $p_v = 0.0$ and the artificial viscosity is $q = 0.0$. The fluid mesh has rectangular 4-node quadrilateral elements; the structural mesh has 2-node line elements. Table 5 shows the numbers of elements and time increments for three cases in this study.

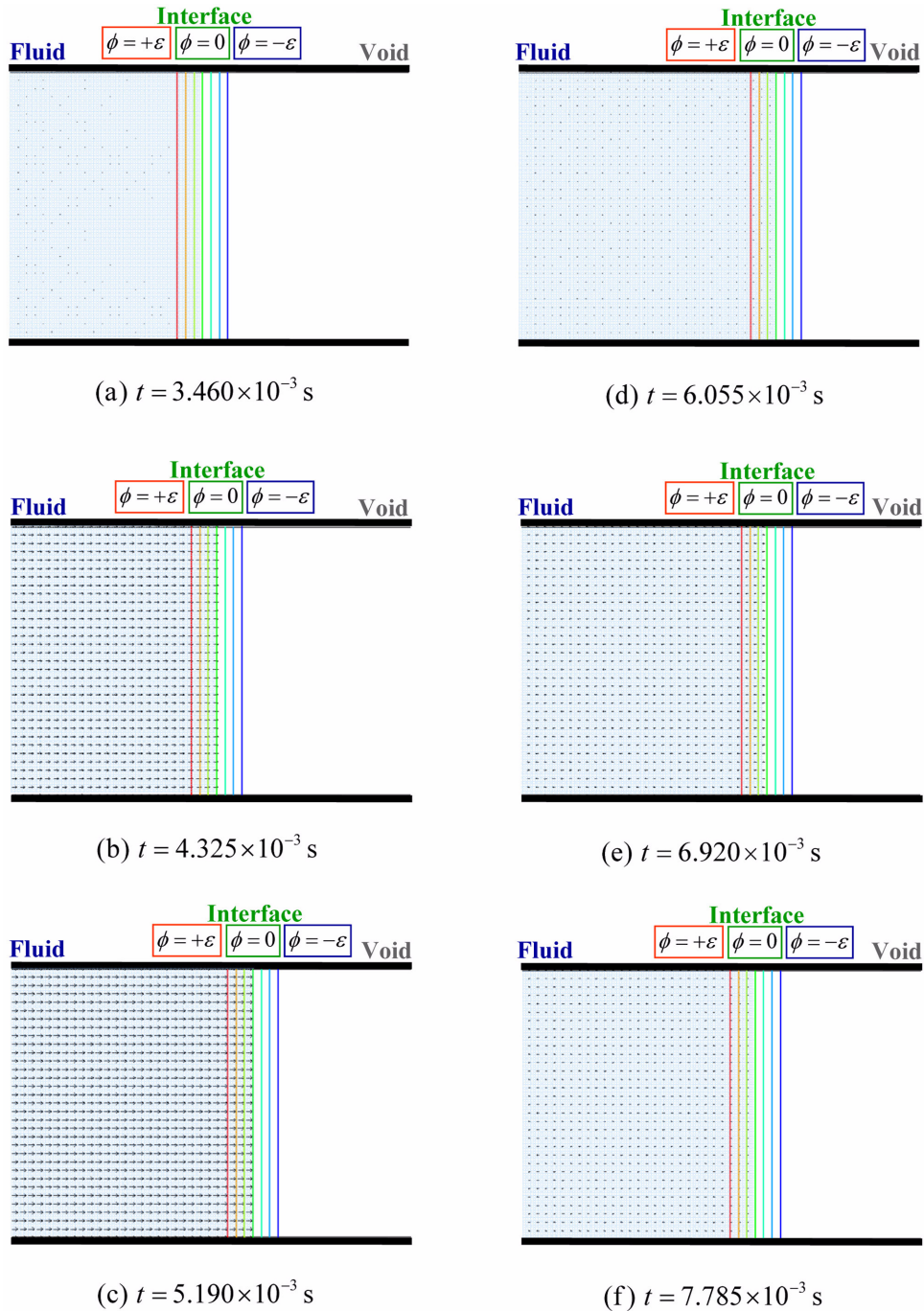


Fig. 14 Velocity vectors near the interface for the water/spring-piston system

Fig. 16 shows time histories of the horizontal (u_1) displacement of the structural bottom point and pressure acting on the structure. The proposed method is compared with reference solutions

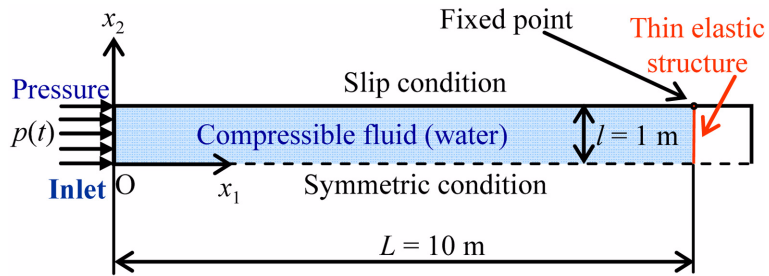
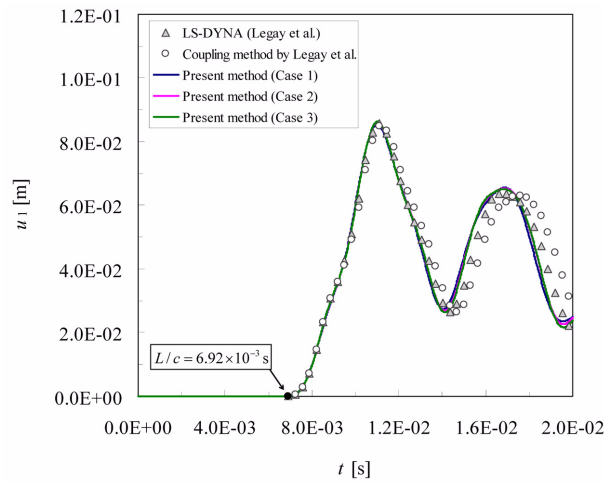
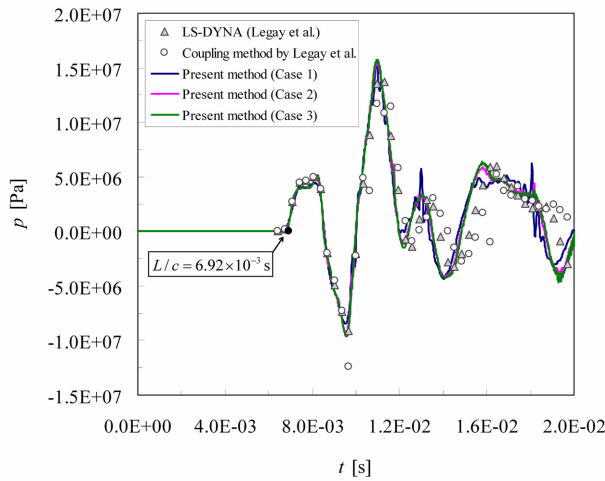


Fig. 15 2D analysis model of a water/thin-elastic-structure system



(a) u_1 displacement



(b) Pressure

Fig. 16 Time histories of u_1 displacement and pressure for the water/thin-elastic-structure system

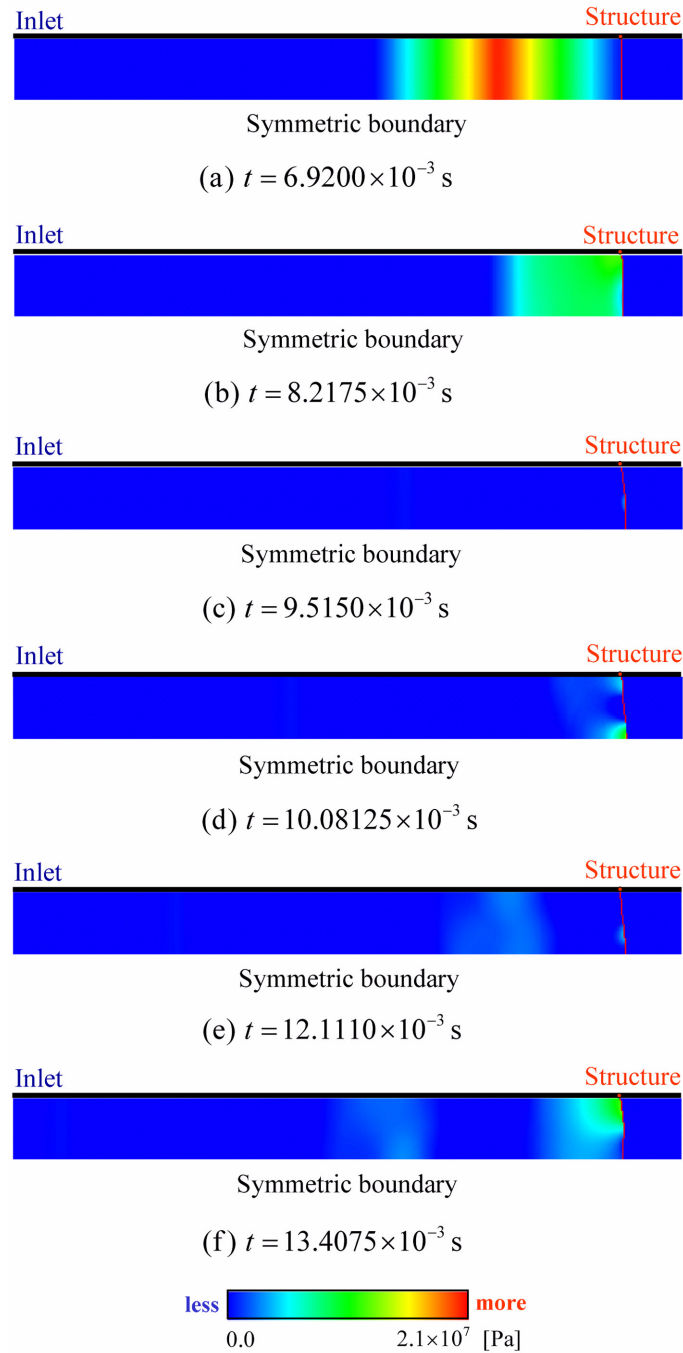


Fig. 17 Pressure contours for the water/thin-elastic-structure system

calculated by the moving ALE mesh-based scheme of LS-DYNA in Legay *et al.* (2006) and by the fixed Eulerian mesh-based scheme of Legay *et al.* (2006). In the Legay scheme, the number of elements used for this problem and the grid convergence are not stated. Because numerical

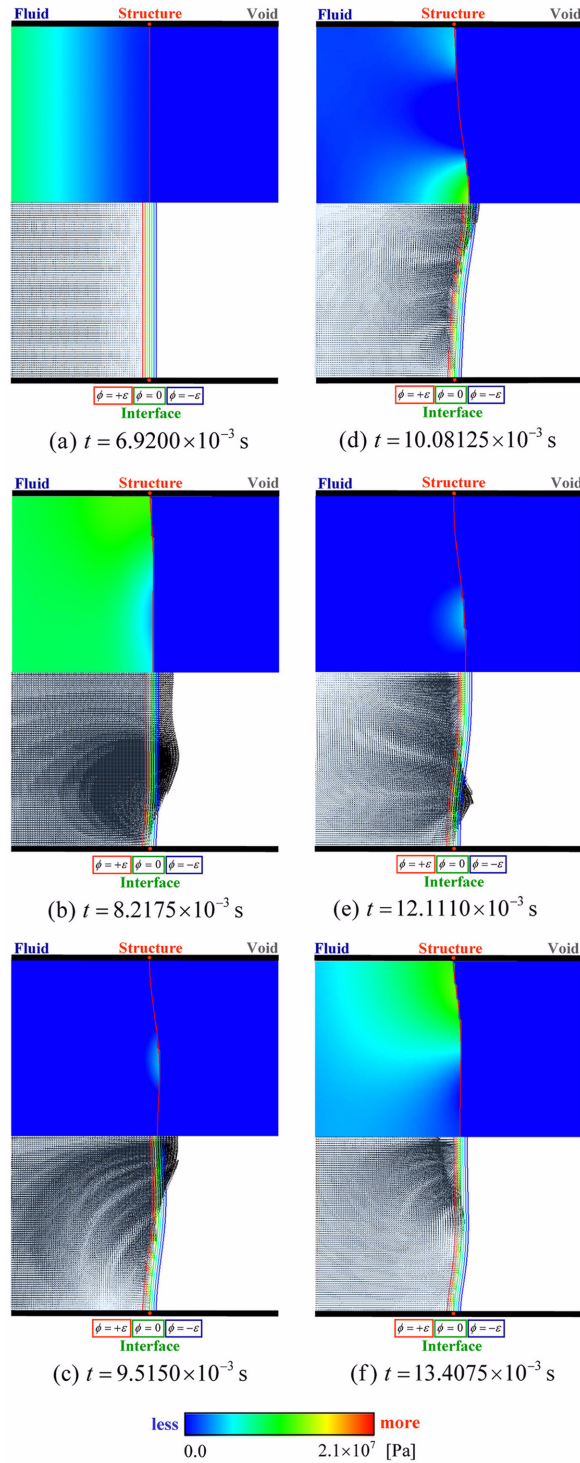


Fig. 18 Flow fields near the interface: pressure contours (upper figures) and velocity vectors (lower figures) for the water/thin-elastic-structure system

oscillations in pressure arise from $t = 1.5 \times 10^{-2}$ s, the number of elements used in the fluid domain is insufficient. The approximate solutions converge near the results for the LS-DYNA scheme when the number of elements changes from Case 1 to Case 3. Increasing the number of elements suppresses the numerical oscillations in pressure.

Fig. 17 shows pressure contours on the fluid mesh for Case 3, and Fig. 18 shows the velocity distribution with isolines of the level set function ($|\phi(x)| \leq \varepsilon$) and pressure contours near the interface for Case 3. After the acoustic wave propagates in the horizontal direction and arrives at the fluid-structure interface, the pressure near the center becomes smaller than the pressure near the fixed points of the structure. Thus, flow forms toward the center of the structure.

6. Large-deformation FSI problem

Fig. 19 shows 2D analysis models of stationary air and a flat airbag. Case 1 is an analysis model for the fluid domain on the inside of the airbag (Fig. 19, upper figure), and Case 2 is an analysis model for the fluid domains on both sides of the airbag (Fig. 19, lower figure). Air flow with high density and high pressure enters the flat airbag from a bottom inlet. We set the geometry of this model and the parameters by referring to the model data of 3D unfolded airbag deployment simulation by Cirak and Radovitzky (2005). A symmetric boundary condition is applied on the left boundary and a slip condition is applied on the bottom boundary except at the inlet. Tables 6 and 7 show the parameters for the compressible inviscid air and a thin elastic structure that appear in this problem. The void pressure is $p_v = 1.0$ atm for Case 1. The parameters for the artificial viscosity are $\alpha_q = 1.0$ and $\beta_q = 1.0$. The fluid mesh has rectangular 4-node quadrilateral elements of 44,032 divisions; the structural mesh has 2-node line elements of 336 divisions. The time increment is $\Delta t = 5.0 \times 10^{-7}$ s.

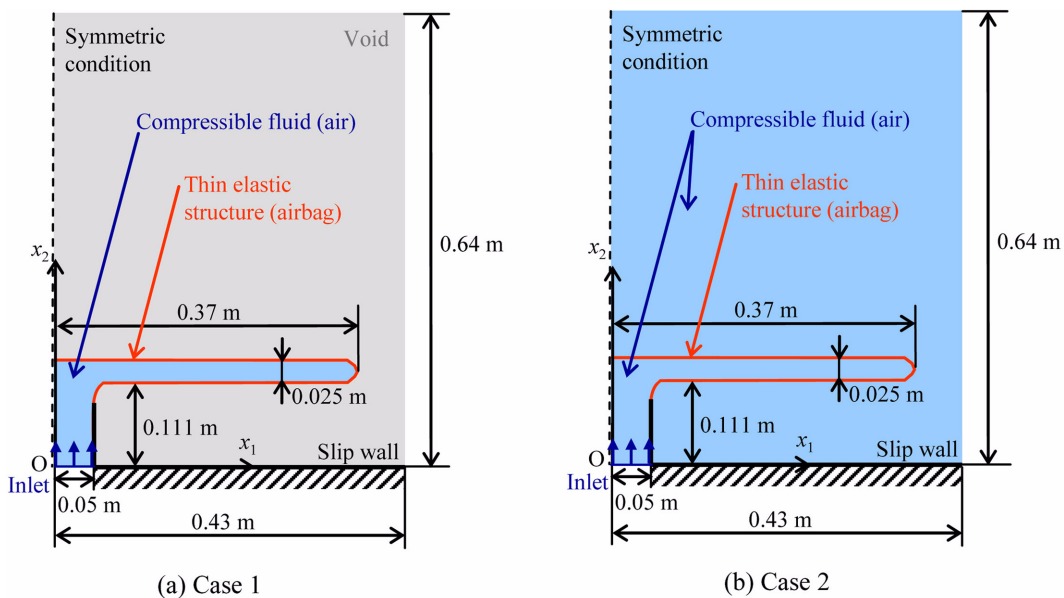


Fig. 19 2D analysis models of an air/thin-elastic-structure (airbag) system

Table 6 Parameters for air (air/thin-elastic-structure system)

Symbol	Meaning	Value
${}^0\rho$	Initial density	1.3 kg/m ³
0p	Initial pressure	1.0 atm
κ	Specific heat ratio	1.4
ρ_{inlet}	Inlet density	16.0 kg/m ³
v_{inlet}	Inlet velocity	73.0 m/s
p_{inlet}	Inlet pressure	12.0 atm

Table 7 Parameters for elastic structure (air/thin-elastic-structure system)

Symbol	Meaning	Value
${}^0\rho$	Initial density	1.0×10^3 kg/m ³
a	Thickness	7.3×10^{-4} m
E	Young's modulus	6.0×10^9 Pa
ν	Poisson's ratio	0.3

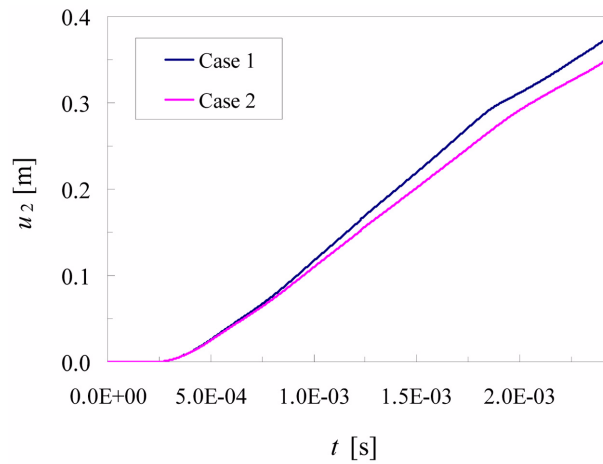
Fig. 20 Time histories of u_2 displacement for the air/thin-elastic-structure (airbag) system

Fig. 20 shows time histories of vertical (u_2) displacement and pressure at the symmetric point of the airbag. Figs. 21 and 22 show the velocity vector distributions with the isolines of the level set function and the pressure contours on the fluid mesh for Cases 1 and 2. When air with high density and high pressure enters the airbag, the airbag inflates because aerodynamic force acts on the top wall, and the side wall moves toward the center of the airbag. In Case 2, the exterior air increases the fluid pressure between the structural elements and the higher pressure prevents the side wall from moving toward the center. As a result, the vertical velocity at the symmetric point of the airbag for Case 2 becomes smaller than for Case 1. The difference in vertical displacement at 2.4 ms is 6.6% (Fig. 20). These results confirm that the present method is capable of solving large-deformation FSI problems.

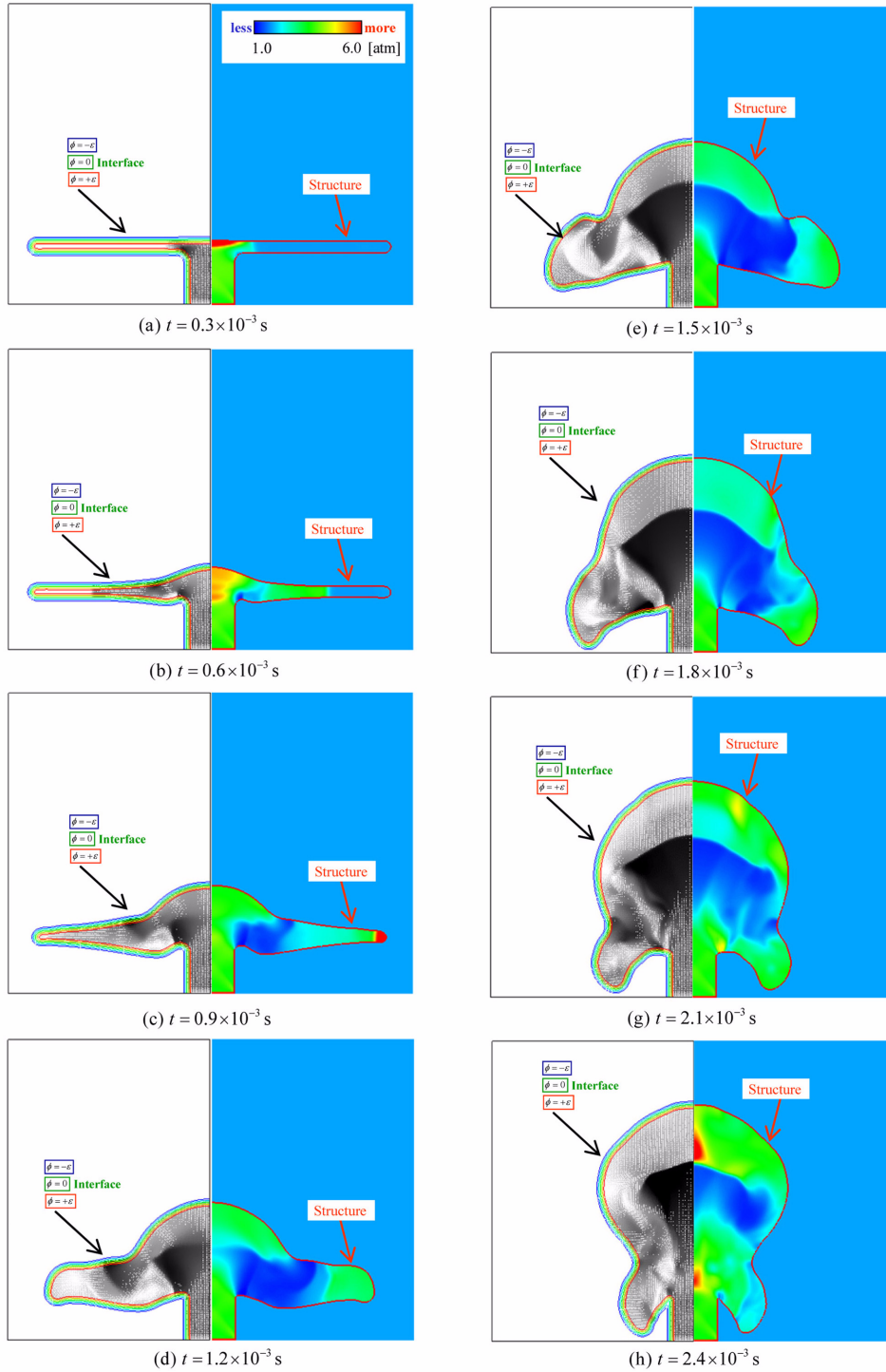


Fig. 21 Flow fields inside airbag for Case 1: velocity vectors (left figures) and pressure contours (right figures) for the air/thin-elastic-structure (airbag) system

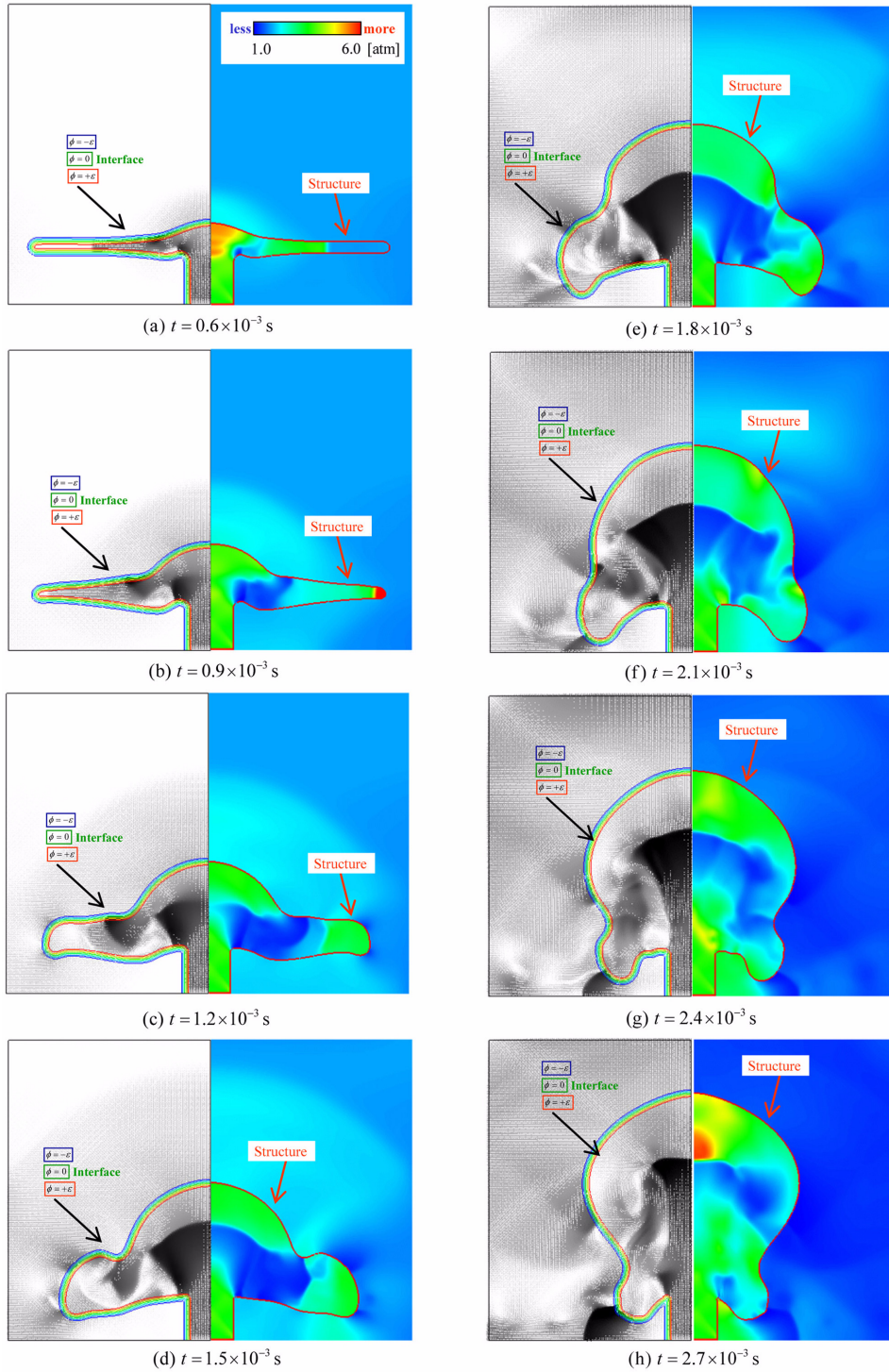


Fig. 22 Flow fields inside airbag for Case 2: velocity vectors (left figures) and pressure contours (right figures) for the air/thin-elastic-structure (airbag) system

7. Conclusions

We proposed a partitioned-solution (iterative-staggered) coupling method based on a fixed Eulerian mesh for large-deformation FSI problems. We used the level set function to describe the complicated geometrical shapes of the fluid-structure interface on the fixed Eulerian mesh, introduced a novel interface-treatment method using virtual nodes with level sets and structural normal velocities, and combined advanced fluid and structure solvers-specifically, the constrained interpolation profile finite element method (CIP-FEM) for the fluid mesh and large-deformable structural elements for the structural mesh. First, we showed that the interface-treatment method using virtual nodes can generate the level set function that represents the property of the signed distance function. Second, for code and calculation verification, we compared the proposed method, the moving ALE mesh-based scheme, and the fixed Eulerian mesh-based scheme of Legay *et al.* (2006) for applicability to finite-deformation FSI problems. Finally, we confirmed that the proposed method is applicable to unfolded airbag deployment simulations.

We plan now to apply the proposed method to folded airbag deployment problems, for which it is necessary to introduce collision detection and repulsive force to handle self-contact of the airbag.

Acknowledgements

We would like to express our gratitude to the late Prof. Hirohisa Noguchi of Keio University for many insightful comments and warm encouragement. This research was supported by a Grant-in-Aid for Young Scientists (B) (24760059) in 2012-2013, Japan Society for the Promotion of Science (JSPS). We gratefully acknowledge this support.

References

- Baajiens, F.P.T. (2001), "A fictitious domain/mortar element method for fluid-structure interaction", *Int. J. Numer. Meth. Fl.*, **35**(7), 743-761.
- Bungartz, H.J. and Schafer, M. (2007), *Fluid-structure interaction, Modeling, Simulation, Optimization*, Springer.
- Cirak, F. and Radovitzky, R. (2005), "A Lagrangian-Eulerian shell-fluid coupling algorithm based on level sets", *Comput. Struct.*, **83**(6-7), 491-498.
- Dvorkin, E., Oñate, E. and Oliver, J. (1988), "On a nonlinear formulation for curved Timoshenko beam elements considering large displacement/rotation increments", *Int. J. Numer. Meth. Eng.*, **26**(7), 1597-1613.
- Enright, D., Fedkiw, R., Ferziger, J. and Mitchell, I. (2002), "A hybrid particle level set method for improved interface capturing", *J. Comput. Phys.*, **183**(1), 83-116.
- Glowinski, R., Pan, T.W. and Periaux, J. (1998), "Distributed Lagrange multiplier methods for incompressible viscous flow around moving rigid bodies", *Comput. Method. Appl. M.*, **151**(1-2), 181-194.
- Hashimoto, G. and Noguchi, H. (2008), "Gas-liquid interface treatment in underwater explosion problem using Moving Least Squares - Smoothed Particle Hydrodynamics", *Interact. Multiscale Mech.*, **1**(2), 251-278.
- Ishihara, D. and Yoshimura, S. (2005), "A monolithic approach for interaction of incompressible viscous fluid and an elastic body based on fluid pressure Poisson equation", *Int. J. Numer. Meth. Eng.*, **64**(2), 167-203.
- Joosten, M.M., Dettmer, W.G. and Peric, D. (2009), "Analysis of the block Gauss-Seidel solution procedure for a strongly coupled model problem with reference to fluid-structure interaction", *Int. J. Numer. Meth. Eng.*, **78**(7), 757-778.
- Lancaster, P. and Salkauskas, K. (1981), "Surfaces generated by moving least squares methods", *Math. Comput.*,

- 37(155), 141-158.
- Legay, A., Chessa, J. and Belytschko, T. (2006), "An Eulerian-Lagrangian method for fluid-structure interaction based on level sets", *Comput. Method. Appl. M.*, **195**(17-18), 2070-2087.
- Mahangare, M., Trepess, D., Blundell, M.V., Hoffmann, J., Freisinger, M. and Smith, S. (2005), "A simulation approach for the early phase of a driver airbag deployment to investigate OoP scenarios", *5th European MADYMO User Conference*, 24-31.
- Makihara, T., Shibata, E. and Tanahashi, T. (1999), "Application of the GSMAC-CIP method to incompressible Navier-Stokes equations at high Reynolds numbers", *Int. J. Comput. Fluid D.*, **12**(3), 301-314.
- Noguchi, H. and Hisada, T. (1993), "Sensitivity analysis in post-buckling problems of shell structures", *Comput. Struct.*, **47**(4), 699-710.
- von Neumann, J. and Richtmyer, R.D. (1950), "A method for the numerical calculation of hydrodynamic shocks", *J. Appl. Phys.*, **21**(3), 232-237.
- Osher, S. and Fedkiw, R. (2003), *Level set method and dynamic implicit surfaces*, Springer.
- Peskin, C.S. and McQueen, D.M. (1989), "A three-dimensional computational method for blood flow in the heart I. immersed elastic fibers in a viscous incompressible fluid", *J. Comput. Phys.*, **81**(2), 372-405.
- Ruff, C., Eichberger, A. and Jost, T. (2006), "Simulation of an airbag deployment in Out-of-Position situation", *5. LS-DYNA Anwenderforum*, 5-16.
- Rugonyi, S. and Bathe, K.J. (2001), "On finite element analysis of fluid flows fully coupled with structural interactions", *CMES*, **2**(2), 195-212.
- Sawada, T. and Hisada, T. (2005), "Overlaying ALE mesh approach to computation of fluid-structure interactions", *Proceedings of the 5th International Conference on Computation of Shell and Spatial Structures, IASS IACM*.
- Sawada, T., Nakasumi, S., Tezuka, A., Fukushima, M. and Yoshizawa, Y. (2009), "Extended-FEM for the solid-fluid mixture two-scale problems with BCC and FCC microstructures", *Interact. Multiscale Mech.*, **2**(1), 45-68.
- Sethian, J.A. (1999), *Level set methods and fast marching methods*, Cambridge University Press.
- Souli, M. and Olovson, L. (2003), "Fluid-structure interaction in LS-DYNA: industrial applications", *4th European LS-DYNA Users Conference*, 35-42.
- Sussman, M., Smereka, P. and Osher, S. (1994), "A level set approach for computing solution to incompressible two-phase flow", *J. Comput. Phys.*, **114**(1), 146-159.
- Takewaki, H., Nishiguchi, A. and Yabe, T. (1985), "The cubic-interpolated pseudo-particle (CIP) method for solving hyperbolic-type equations", *J. Comput. Phys.*, **61**(2), 261-268.
- Wall, W.A. and Ramm, E. (1998), "Fluid-structure interaction based upon a stabilized (ALE) finite element method", *Computational Mechanics (World Congress), New Trends and Applications*, 1-20.
- Wang, X. and Liu, W.K. (2004), "Extended immersed boundary method using FEM and RKPM", *Comput. Meth. Appl. M.*, **193**(12-14), 1305-1321.
- Wilkins, M.L. (1980), "Use of artificial viscosity in multidimensional fluid dynamics calculation", *J. Comput. Phys.*, **36**(3), 281-303.
- Zhang, H., Raman, S., Gopal, M. and Han, T. (2004), "Evaluation and comparison of CFD integrated airbag models in LS-DYNA, MADYMO and PAM-CRASH", *SAE International*, 2004-01-1627, 1-13.
- Zhang, L., Gerstenberger, A., Wang, X. and Liu, W.K. (2004), "Immersed finite element method", *Comput. Method. Appl. M.*, **193**(21-22), 2051-2067.
- Zhang, Q. and Hisada, T. (2001), "Analysis of fluid-structure interaction problems with structural buckling and large domain changes by ALE finite element method", *Comput. Method. Appl. M.*, **190**(48), 6341-6357.
- Zhang, X., Chen, J.S. and Osher, S. (2008), "A multiple level set method for modeling grain boundary evolution of polycrystalline materials", *Interact. Multiscale Mech.*, **1**(2), 191-209.